Estimated principal components of deformation tensors derived from GPS measurements under assumption of both independent and correlated tensor observations (case study: Zagros mountains, Iran)

K. Moghtased-Azar[a], E. W. Grafarend[b], F. Tavakoli[c], H. R. Nankali[c]

[a] *Department of Surveying Engineering, Faculty of Civil Engineering, University of Tabriz, 29 Bahman Boulevard, P.O. Box 51666-16471, Tabriz, Iran*
[b] *Institute of Geodesy, Geschwister-Scholl-Str. 24D, P.O. Box D-70174, Stuttgart, Germany*
[c] *National Cartographic Centre (NCC) of Iran, Meraj Ave., Azadi Sq., P.O. Box 13185 1684, Tehran, Iran*

Abstract

In this contribution, the procedure of estimation of principal components of deformation tensors in the presence of both independent and correlated tensor observations of displacement field is presented. This approach is based upon the intrinsic method which assumed the Earth as two-dimensional Riemmannian manifold ($\mathbb{M}^2$) embedded in the ambient space (three-dimensional Euclidean space $\mathbb{E}^3$) at various time instants. The context is divided into two parts: In the first, we considered independent random vectors and in the second step we considered correlations between repeated measurements. Then, the covariance components between tensor elements are estimated by Helmert estimator, based on prior information of variance components. As a case study, both assumption, are applied to the estimation of principal components of deformation rate tensor observations in Zagros region. The latest available continuous GPS data around the region, when this research is undertaken, was from January 2006 through January 2009. Due to the sparsity of the data between the January 2006 through January 2007, which could effect the construction of the Earths surface as regularized and graded M2 at continuous time instants, we have chose the daily solutions between January 2007 through January 2009. In this region, the invariants of deformation rates tensors within 95matrix and, (b) after estimation of covariance matrix. The related linear hypothesis test has documented larger confidence regions for the active areas, after estimation of (Co)variance components. They lead to a statement of caution when dealing with data concerning extension and contraction, as well as the orientation of principal stresses. Further detailed analysis of the results is also performed with respect to geodynamical and statistical aspects.

Keywords: Random tensor, Principal components , (Co)variance component estimation

1. Introduction

In this contribution, in the presence of errors in measuring a random displacement field (under the normal distribution assumption of displacement field), stochastic behaviors of principal components of deformation tensors (strain tensor and TCC) are discussed. We divided the context into two parts: In the first, we considered *independent* random vectors of repeated tensor measurements. In the second step, we considered *correlations* between repeated measurements. Then, covariance components between tensor elements by Helmert estimator, based on prior information of variance components, are estimated. The possible recorded confi-

Email addresses: moghtased@tabrizu.ac.ir (K. Moghtased-Azar), grafarend@gis.uni-stuttgart.de (E. W. Grafarend), farokh.tavakoli@ncc.org.ir (F. Tavakoli), nankali@ncc.org.ir (H. R. Nankali)

dence regions for eigenspace components based upon both contexts (in multivariate data analysis), could clarify the impact of (co)variance components estimation in statement of caution when dealing with data concerning extension and contraction, as well as the orientation of principal stresses.

In the second part of the paper, we briefly review the intrinsic method for surface deformation analysis of the Earth. In the third part, we deal with the statistical induction of the principal components of deformation tensors, in intrinsic method. In the fourth part, the proposed models are applied by a numerical example to geodetic network consisting of 11 permanent GPS stations around the Zagros region, which has nearly daily solutions (in ITRF 2005) for the period January 2007 through January 2009. Further detailed analysis of the results is also performed with respect to geodynamic and statistical aspects.

2. Surface deformation

2.1. Deterministic Model

In this method, the Earth's surface is considered as differentiable surface (in which tangent space is equipped with an inner product) $\mathbb{M}^2$ embedded in $\mathbb{E}^3$. Deformation of the Earth's surface is expressible by mapping of the *left* surface $\{\mathbb{M}_l^2, G_{\Lambda\Phi}\}$, in the reference time with associated standard positive definite metric $\mathbf{G} := [G_{\Lambda\Phi}]$, onto the *right* surface $\{\mathbb{M}_r^2, g_{\lambda\phi}\}$ in the current time with defined metric tensor $\mathbf{g} := [g_{\lambda\phi}]$. We assumed that this mapping is single valued and has *continuous* partial derivatives with respect to their arguments. Namely, each point $m \in \mathbb{M}_r^2$ is the *unique inverse* of the other in a neighborhood of the material point $M \in \mathbb{M}_l^2$, which implies *indestructibility of matter* as well as *impenetrability of matter*.

On the curvilinear coordinates of the $\{\Lambda, \Phi\} \in \mathbb{M}_l^2$ and $\{\lambda, \phi\} \in \mathbb{M}_r^2$, *Gaussian moving frames* could be constructed in the forms

$$\begin{gathered}\text{Reference frame of type}\\ \text{Gauss on } \mathbb{M}_l^2\\ \{\mathbf{G}_1, \mathbf{G}_2, \mathbf{G}_3|\Lambda, \Phi\}\\ \mathbf{G}_1 := \mathbf{X}_{,\Lambda},\ \mathbf{G}_2 := \mathbf{X}_{,\Phi}\\ \mathbf{G}_3 := \frac{\mathbf{G}_1\times\mathbf{G}_2}{|\mathbf{G}_1\times\mathbf{G}_2|}\end{gathered} \qquad (1)$$

$$\begin{gathered}\text{Reference frame of type}\\ \text{Gauss on } \mathbb{M}_r^2\\ \{\mathbf{g}_1, \mathbf{g}_2, \mathbf{g}_3|\lambda, \phi\}\\ \mathbf{g}_1 := \mathbf{x}_{,\lambda},\ \mathbf{g}_2 := \mathbf{x}_{,\phi}\\ \mathbf{g}_3 := \frac{\mathbf{g}_1\times\mathbf{g}_2}{|\mathbf{g}_1\times\mathbf{g}_2|}\end{gathered}$$

where $\mathbf{X}(\Lambda, \Phi)$ and $\mathbf{x}(\lambda, \phi)$ are the placement vectors in left and right surfaces, respectively. Then, metric tensors in curvilinear coordinates for each point on the surfaces could be written in the forms $G_l := [G_{\Lambda\Phi}] =< \mathbf{G}_\Lambda, \mathbf{G}_\Phi >$ vs. $G_r := [g_{\lambda\phi}] =< \mathbf{g}_\lambda, \mathbf{g}_\phi >$. Furthermore, components of the strain tensor at a point are related to the curvilinear derivatives of the displacement vector $\mathbf{u} = \mathbf{x} - \mathbf{X}$ (Grafarend and Voosoghi 2003)

$$\begin{gathered}E_l = \tfrac{1}{2}(< \mathbf{u}_{,\Lambda}, \mathbf{u}_{,\Phi} > + < \mathbf{u}_{,\Lambda}, \mathbf{G}_\Phi > + < \mathbf{G}_\Lambda, \mathbf{u}_{,\Phi} >)\\ \text{vs.}\\ E_r = \tfrac{1}{2}(< \mathbf{u}_{,\lambda}, \mathbf{u}_{,\phi} > + < \mathbf{u}_{,\phi}, \mathbf{g}_\lambda > + < \mathbf{g}_\phi, \mathbf{u}_{,\lambda} >)\end{gathered} \qquad (2)$$

where $\mathbf{u}_{,\Lambda}$ and $\mathbf{u}_{,\phi}$ are the first-order partial derivatives of the displacement vector with respect to the left and right curvilinear coordinates. Solving the left and right *general eigenvalue-eigenvector problems* of the pairs $\{E_l, G_l\}$ and $\{E_r, G_r\}$, yield

$$\begin{gathered}\Lambda_{1,2} = \tfrac{1}{2}(\mathrm{tr}(E_l G_l^{-1}) \pm \sqrt{(\mathrm{tr}(E_l G_l^{-1}))^2 - 4\mathrm{det}(E_l G_l^{-1})}\\ \cos\Psi_l = \frac{f^1_{lm}}{\|\mathbf{f}_{lm}\|}\ \ ;\ \ \Psi_l \in [-\tfrac{\pi}{2}, \tfrac{\pi}{2}]\\ \lambda_{1,2} = \tfrac{1}{2}(\mathrm{tr}(E_r G_r^{-1}) \pm \sqrt{(\mathrm{tr}(E_r G_r^{-1}))^2 - 4\mathrm{det}(E_r G_r^{-1})}\\ \cos\Psi_r = \frac{f^1_{rm}}{\|\mathbf{f}_{rm}\|}\ \ ;\ \ \Psi_r \in [-\tfrac{\pi}{2}, \tfrac{\pi}{2}]\end{gathered} \qquad (3)$$

where $\{\Lambda_1, \Lambda_2\}$ and $\{\lambda_1, \lambda_2\}$ are the principal stretches, where a deformation portrait with a positive eigenvalue is refereed to the *extension*, with a negative eigenvalue as *compression*. In Eq. (3), orientation of principal eigenvectors, are represented by Ψ_l and Ψ_r, respectively. These angles are conventionally measured counterclockwise with respect to the east directions. The principal eigenvectors are represented by $\|\mathbf{f}_{lm}\|^2 = \max\{\|\mathbf{f}_l^1\|, \|\mathbf{f}_l^2\|\}$ and $\|\mathbf{f}_{rm}\|^2 = \max\{\|\mathbf{f}_r^1\|, \|\mathbf{f}_r^2\|\}$, re-

spectively. However, the eigenvectors could be represented using *nonlinear functions* of the components of deformation tensors, metric tensors and principal stretches by

$$\begin{array}{c} \mathbf{f}_l^{\Psi} := \mathcal{F}(E_l, G_l, \Lambda_{\Psi}) \ , \ \forall \Psi \in \{1,2\} \\ \text{vs.} \\ \mathbf{f}_r^{\Psi} := \mathcal{F}(E_r, G_r, \lambda_{\psi}) \ , \ \forall \Psi \in \{1,2\} \end{array} \tag{4}$$

where $\mathbf{f}_l^{\Psi}$ and $\mathbf{f}_r^{\Psi}$ are the left and right eigencolumns (Moghtased-Azar and Grafarend 2009). The off-diagonal elements of the metric tensors of the pairs $\{E_l, G_l\}$ and $\{E_r, G_r\}$ are not zeros. They set up intricate relations between elements of deformation tensors and eigenspace components (see Eqs. (3) and (4)). Hence, in conformity with standard lemma of matrix algebra both pairs of matrices $\{E_l, G_l\}$ or $\{E_r, G_r\}$ can be simultaneously diagonalized, metric matrices being the unit matrices. Moreover, we make this simplified assumption that off-diagonal elements of the G_l as well as of the G_r vanish. The new frame, namely *Cartan reference frame* is represented by:

$$\begin{array}{c} \text{Reference frame of type} \\ \text{Cartan on } \mathbb{M}_l^2 \\ \{\mathbf{C}_1, \mathbf{C}_2, \mathbf{C}_3 | \Lambda, \Phi\} \\ \mathbf{C}_1 = \frac{G_1}{|G_1|} = \frac{G_1}{\sqrt{G_{11}}}, \mathbf{C}_2 = \frac{G_2}{|G_2|} = \frac{G_2}{\sqrt{G_{22}}} \\ \mathbf{C}_3 := \frac{\mathbf{C}_1 \times \mathbf{C}_2}{|\mathbf{C}_1 \times \mathbf{C}_2|} \\ \text{vs.} \\ \text{Reference frame of type} \\ \text{Cartan on } \mathbb{M}_r^2 \\ \{\mathbf{c}_1, \mathbf{c}_2, \mathbf{c}_3 | \lambda, \phi\} \\ \mathbf{c}_1 = \frac{g_1}{|g_1|} = \frac{g_1}{\sqrt{g_{11}}}, \mathbf{c}_2 = \frac{g_2}{|g_2|} = \frac{g_2}{\sqrt{g_{22}}} \\ \mathbf{c}_3 := \frac{\mathbf{c}_1 \times \mathbf{c}_2}{|\mathbf{c}_1 \times \mathbf{c}_2|} \end{array} \tag{5}$$

Afterwards, in Cartan reference frames, deformation tensors associated with metric tensors will change to the E_l'' and E_r''. The eigenvalues have no change due to the transformations. However, the orientation parameters in two cases are different and could be represented by (Moghtased-Azar and Grafarend, 2009)

$$\begin{array}{c} \tan\Theta_l = \frac{\sqrt{\det\,[G_l]}}{G_{11} + G_{12}\tan\Psi_l} \tan\Psi_l \\ \text{vs.} \\ \tan\Theta_r = \frac{\sqrt{\det\,[G_r]}}{g_{11} + g_{12}\tan\Psi_r} \tan\Psi_r \end{array} \tag{6}$$

in which the orientation parameters of the maximum principal axes of the deformation tensors in Gaussian moving frames are represented by $\{\Psi_l, \Psi_r\}$, while those parameters of the transformed deformation tensors in Cartan moving frames are illustrated by $\{\Theta_l, \Theta_r\}$.

Due to the mapping from $\mathbb{M}_l^2$ to $\mathbb{M}_r^2$, which is implied by the deformation process, the TCC as a second deformation tensor would be changed. In accordance with definition of strain tensors (Eq. 2), TCC could be illustrated by

$$\begin{array}{c} K_{\Lambda\Phi} = - < \mathbf{w}_{,\Lambda}, \mathbf{G}_{\Phi} > - < \mathbf{w}_{,\Lambda}, \mathbf{u}_{,\Phi} > - < \mathbf{u}_{,\Phi}, \mathbf{G}_{3,\Lambda} > \\ \text{vs.} \\ k_{\lambda\phi} = - < \mathbf{w}_{,\lambda}, \mathbf{g}_{\phi} > - < \mathbf{w}_{,\lambda}, \mathbf{u}_{,\phi} > - < \mathbf{u}_{,\phi}, \mathbf{g}_{3,\lambda} > \end{array} \tag{7}$$

where $\mathbf{w} = \mathbf{G}_3 - \mathbf{g}_3$ is defined as the difference of a unit normal vector on $\mathbb{M}_l^2$ and a unit normal vector on $\mathbb{M}_r^2$. Therefore, deformation of the $\mathbb{M}^2$ could be completely specified by the changing of metric tensor and TCC, which TCC is responsible for detection of vertical displacements of the $\mathbb{M}^2$.

2.2. Stochastic Model

2.2.1. In the context of independent observations

According to the measurement axiom, a measured symmetric rank-two tensor is random and tensor-valued *Gauss-Laplace* normally distributed over $\mathbb{R}^{2\times 2}$. Let us consider the elements of symmetric random deformation tensor of type rank-two, in Cartan frame by $E'' = [E_{ij}''] \in \mathbb{R}^{2\times 2}$, where $\text{vech}\,(E'') = [E_{11}''\ E_{12}''\ E_{22}'']^{\mathrm{T}} =: \tilde{\mathbf{y}}'' \in \mathbb{R}^{3\times 1}$ denotes to the half-vectorization of E''. For a symmetric deformation tensor E'', the problem of principal components analysis versus synthesis is summarized by (Xu and Grafarend 1996)

$$\begin{array}{c} \boldsymbol{\xi} = \begin{bmatrix} \Lambda_1 \\ \Lambda_2 \\ \Theta \end{bmatrix} = \frac{1}{2} \begin{bmatrix} E_{11}'' + E_{22}'' + \sqrt{(E_{11}'' - E_{22}'')^2 + 4E_{12}''} \\ E_{11}'' + E_{22}'' - \sqrt{(E_{11}'' - E_{22}'')^2 + 4E_{12}''} \\ \arctan \frac{2E_{12}''}{E_{11}'' - E_{22}''} \end{bmatrix} \\ \text{vs.} \\ \begin{bmatrix} f_1 \\ f_2 \\ f_3 \end{bmatrix} = \begin{bmatrix} E_{11}'' \\ E_{12}'' \\ E_{22}'' \end{bmatrix} = \begin{bmatrix} \Lambda_1 \cos^2\Theta + \Lambda_2 \sin^2\Theta \\ \frac{1}{2}(\Lambda_2 - \Lambda_1)\sin 2\Theta \\ \Lambda_1 \sin^2\Theta + \Lambda_2 \cos^2\Theta \end{bmatrix} \end{array} \tag{8}$$

Assume that n independent samples of E'' namely $E_1'', E_2'', \ldots, E_n''$ have been observed directly or indirectly determinedbeen either observed directly or determined indirectly by other measurements, e.g., GPS measurements, and vectorized into the forms $\tilde{\mathbf{y}}_{\mathbf{1}}'', \tilde{\mathbf{y}}_{\mathbf{2}}'', \ldots, \tilde{\mathbf{y}}_{\mathbf{n}}''$. Here, we design an array of vectorized tensor coordinates

$\tilde{y}''_1 := E''_1,\ \tilde{y}''_2 := E''_2,\ \tilde{y}''_3 := E''_3$ indexed to the number of samples

$$\mathbf{Y}'' := [\tilde{\mathbf{y}}''_{\mathbf{1}}, \tilde{\mathbf{y}}''_{\mathbf{2}}, \ldots, \tilde{\mathbf{y}}''_{\mathbf{n}}] = \begin{bmatrix} \tilde{y}''_{1.1} & \ldots & \tilde{y}''_{1.n} \\ \tilde{y}''_{2.1} & \ldots & \tilde{y}''_{2.n} \\ \tilde{y}''_{3.1} & \ldots & \tilde{y}''_{3.n} \end{bmatrix} \ ;\ \mathbf{Y}'' \in \mathbb{R}^{3\times n} \tag{9}$$

Let us suppose a special nonlinear multivariate *Gauss-Markov* model for sampling the eigenspace synthesis

$$\mathbf{Y}'' = F(\boldsymbol{\xi})\mathbf{1}^{\mathrm{T}} + \bar{\mathbf{E}} \Rightarrow \mathrm{E}\{\mathbf{Y}''\} = F(\boldsymbol{\xi})\mathbf{1}^{\mathrm{T}} \tag{10}$$

where $\mathbf{1}$ denotes the $n \times 1$ *summation vector* with all its entries being unity, $\bar{\mathbf{E}}$ displays residual vectors and $\mathrm{E}\{\mathbf{Y}''\}$ denotes to first moments. The linearization process using the *Taylor* expansion, yields

$$F(\boldsymbol{\xi}) = F(\boldsymbol{\xi}_0) + J(\boldsymbol{\xi}_0)(\boldsymbol{\xi} - \boldsymbol{\xi}_0) + O[(\boldsymbol{\xi} - \boldsymbol{\xi}_0) \otimes (\boldsymbol{\xi} - \boldsymbol{\xi}_0)] \tag{11}$$

where $\Delta\boldsymbol{\xi} = \boldsymbol{\xi} - \boldsymbol{\xi}_0$. Hence, we establish a special linearized multivariate *Gauss-Markov* model for the eigenspace synthesis

$$\mathbf{Y}'' = F(\boldsymbol{\xi}_0)\mathbf{1}^{\mathrm{T}} + [J(\boldsymbol{\xi}_0)\Delta\boldsymbol{\xi}]\mathbf{1}^{\mathrm{T}} + \mathbf{E} \tag{12}$$

which is in vectorized form (Cai et al. 2005)

$$\begin{aligned} \mathrm{vec}\ \mathbf{Y}'' &= \mathrm{vec}\ \mathbf{Y}''_0 + A\Delta\boldsymbol{\xi} + \mathrm{vec}\ \mathbf{E} \\ \mathrm{vec}\ \mathbf{Y}''_0 &= \mathbf{1} \otimes F(\boldsymbol{\xi}_0)\ ;\ A = 1 \otimes J(\boldsymbol{\xi}_0) \end{aligned} \tag{13}$$

where first moment could be denoted by $A\Delta\boldsymbol{\xi} + \mathrm{vec}\ \mathbf{E} + \mathrm{vec}\ \mathbf{Y}''_0 = \mathrm{E}\{\mathrm{vec}\ \mathbf{Y}''\}$; $\mathrm{vec}\ \mathbf{Y}'' \in \mathbb{R}^{3n\times 1}$ and second moment is $\mathrm{D}\{\mathrm{vec}\ \mathbf{Y}''\} = \mathrm{blkdiag}\ [Q_{\mathbf{y}''_1}, Q_{\mathbf{y}''_2}, \ldots, Q_{\mathbf{y}''_n}] = Q_{\mathbf{Y}''}$; $\mathrm{rank}\ Q_{\mathbf{Y}''} = 3n$, in which blkdiag denotes a block diagonal matrix of $Q_{\mathbf{y}''_i} \in \mathbb{R}^{3\times 3}$ independent covariance matrices. With the assumption of independent observation of random tensor, estimation of the $\Delta\hat{\boldsymbol{\xi}}$ could be given by

$$\begin{aligned} \Delta\hat{\boldsymbol{\xi}} = \hat{\boldsymbol{\xi}} - \boldsymbol{\xi}_0 &= (A^{\mathrm{T}}Q^{-1}_{\mathbf{Y}''}A)^{-1}A^{\mathrm{T}}Q^{-1}_{\mathbf{Y}''}(\mathrm{vec}\ \mathbf{Y} - \mathrm{vec}\ \mathbf{Y}''_0); \\ \mathrm{D}\{\hat{\boldsymbol{\xi}}\} = Q_{\hat{\boldsymbol{\xi}}} &= (A^{\mathrm{T}}Q^{-1}_{\mathbf{Y}''}A)^{-1} \end{aligned} \tag{14}$$

where the dispersion matrix of the unknown parameters expressed by $\mathrm{D}\{\hat{\boldsymbol{\xi}}\}$. Then, the vectorized form of the estimated observations, namely $\mathrm{vec}(\hat{\mathbf{Y}}'')$, and vectorized form of the estimated residual vectors, $\mathrm{vec}(\hat{\mathbf{E}})$, are given by:

$$\mathrm{vec}(\hat{\mathbf{Y}}'') = A(A^{\mathrm{T}}Q^{-1}_{\mathbf{Y}''}A)^{-1}A^{\mathrm{T}}Q^{-1}_{\mathbf{Y}''}\mathrm{vec}(\mathbf{Y}'') \tag{15}$$

$$\mathrm{vec}(\hat{\mathbf{E}}) = \mathrm{vec}(\mathbf{Y}'') - \mathrm{vec}(\hat{\mathbf{Y}}'') = D_{(\sigma)}\ \mathrm{vec}(\mathbf{Y}'') \tag{16}$$

$$D_{(\sigma)} = (\mathrm{I} - A(A^{\mathrm{T}}Q^{-1}_{\mathbf{Y}''}A)^{-1}A^{\mathrm{T}}Q^{-1}_{\mathbf{Y}''}) \tag{17}$$

2.3. In the context of dependent observations

In previous section, we assumed tensor observations are independent. Hence, the covariance matrix of observations is partly known, and incomplete knowledge of the covariance matrix of the observations may lead to unreliable results. An appropriate statistical model is needed to arrive at a proper description of the estimator quality. In this section, we aim to estimate the full covariance matrix for the observations, using Helmert method.

Hence, partitioning the full covariance matrix of measurements into p groups of matrices yields

$$\mathrm{D}\{\mathrm{vec}(\mathbf{Y}'')\} = \sum_{j=1}^{\bar{p}} Q_{jj}\sigma_j^2 + \sum_{j=1}^{\bar{p}-1}\sum_{k=j+1}^{\bar{p}} Q_{jk}\sigma_{jk} \tag{18}$$

with $p = \frac{\bar{p}(\bar{p}+1)}{2}$ variance and covariance components. Here, we assumed that symmetric matrix Q_{jk} is known and has order $3n \times 3n$. We can design an array consisting of matrices Q_{jk} by $Q := [Q_{11}\ \ Q_{12}\ \ Q_{22}\ \ Q_{13}\ \ Q_{23}\ \ Q_{33}\ \ \ldots\ \ Q_{\bar{p}-1\bar{p}}\ \ Q_{\bar{p}\bar{p}}] = [Q_1\ \ Q_2\ \ \ldots\ \ Q_p]$ in which $\mathrm{D}\{\mathrm{vec}(\mathbf{Y}'')\}$ is positive definite and its diagonal elements *priority* are given. We consider that $\bar{p}$ second moments σ_j^2 of type variance and the $\frac{\bar{p}(\bar{p}-1)}{2}$ second moments of type covariance are unknown, which are collected in the array $\boldsymbol{\sigma} = \left[\sigma_1^2\ \ \sigma_{12}\ \ \sigma_2^2\ \ \sigma_{13}\ \ \ldots\sigma_{23}\ \ \sigma_3^2\ \ \ldots\ \ \sigma_{\bar{p}-1\bar{p}}\ \ \sigma_{\bar{p}}^2\right]^{\mathrm{T}}$. Then, Eq.(15), will be represented by

$$Q_{\mathbf{Y}''} = \sum_{j=1}^{p} Q_j\sigma_j \tag{19}$$

Now, let us set up an estimator of Helmert type, based upon the idea that least squares residuals $\mathrm{vec}(\hat{\mathbf{V}}_{\mathbf{Y}''})$ are invariant with respect to the transformation $\mathrm{vec}(\mathbf{Y}'') \rightarrow \mathrm{vec}(\mathbf{Y}'') + A\,\boldsymbol{\xi}$. The shifting variate is the squared norm

of the least-squares residuals. Its expectation, through Eqs .(15), can be given as

$$\mathrm{E}\{\mathrm{vec}(\hat{\mathbf{V}}_{\mathbf{Y}''})^{\mathrm{T}} Q_{\mathbf{Y}''}^{-1} \mathrm{vec}(\mathbf{V}_{\mathbf{Y}''})\} = \mathrm{tr}(D_{(\sigma)}^{\mathrm{T}} Q_{\mathbf{Y}''}^{-1} D_{(\sigma)} Q_{\mathbf{Y}''}) \tag{20}$$

Grafarend et al. (1980) used a block-structured covariance matrix: $Q_{\mathbf{Y}''} = \sum_{j=1}^{p} Q_j \sigma_j$ with the multinomial inverse of the form : $Q_{\mathbf{Y}''}^{-1} = \sum_{i=1}^{p} K_i \sigma_i$. He gave a simple example how to obtain K_i's. When the covariance matrix $\mathrm{D}\{\mathrm{vec}(\mathbf{Y}'')\}$ has a block-diagonal structure one can also simply obtain K_i's. Substituting these two terms in the proceeding equation can be written in a compact form as $\mathrm{E}\{\mathbf{q}\} = H\boldsymbol{\sigma}$ in which

$$h_{ij} = \mathrm{tr}(D_{(\sigma)}^{\mathrm{T}} K_i D_{(\sigma)} Q_j) \quad , \quad i,j = 1,\ldots,p \tag{21}$$

$$q_i = \mathrm{vec}(\hat{\mathbf{V}}_{\mathbf{Y}''})^{\mathrm{T}} K_i \ \mathrm{vec}(\hat{\mathbf{V}}_{\mathbf{Y}''}) \tag{22}$$

where $H \in \mathbb{R}^{p\times p}$ (Helmert matrix) and $\mathbf{q} \in \mathbb{R}^{p\times 1}$. If H is regular, an unbiased estimator of (co)variance components reads

$$\hat{\boldsymbol{\sigma}} = H^{-1}\boldsymbol{q} \tag{23}$$

If the Helmert matrix is a regular matrix then it has the block structure and estimated variances are unbiased and invariant (Grafarend et al. 1980).

3. Tectonics of Zagros Mountains

In western Iran, the main feature of the continental collision is the Zagros range, which extends for about 1500 km along the NW-SE trending boundary between the Arabian plate and Central Iran block. The Zagros Mountains (or Fold-Thrust Belt) are actively deforming due to the oblique continental collision between Arabian and Eurasian plates. A relatively dense GPS network (distance between neighbor stations vary from 190 to 400 km) which is covered the Zagros in the Iranian part, proves this collision is still active and the resulting deformation is distributed non-uniformly in the country, mainly taken up in the major mountain belts like Alborz and Zagros (Nilforoushan et al. 2003).

The region is divided into three major areas, the North Zagros, the Central Zagros, and the region of the Kazerun fault system separating North and Central Zagros. In the North Zagros the deformation is divided among reverse faults (which indicative of shortening of the crust) and right-lateral strike-slip motion on the Main Recent Fault (MRF). In the Central Zagros, the deformation is supplied largely in the south along the Persian Gulf. In Central Zagros, the fold trends turn to EW direction.

The Kazerun Fault is a NS trending fault zone, which obliquely truncates the NW (the North Zagros) and SE (the Central Zagros) trending Zagros Fold-Thrust Belt. its deformation regime is partitioned into shortening and strike-slip on different faults. The earthquake focal mechanisms on the Kazerun Fault system show right-lateral strike-slip motion. Fig. 1 illustrates the significant faults of Zagros range. Talebian and Jackson (2004) have proposed a tectonical model constrained by earthquake slip vector directions to describe schematically how the Zagros accommodates presently the Arabia-Eurasia collision.

In the North Zagros (Borujerd-Dezful), oblique shortening is partitioned into right-lateral strike-slip on MRF and orthogonal shortening. In the Central Zagros (Bandar Abbas) no strike-slip is necessary, as the shortening is parallel to the overall convergence. The zone around the Kazerun Fault system is where the transition between these two regimes occurs, with anticlockwise rotating strike-slip faults allowing an along-strike extension between Bandar Abbas and Dezful (see Fig. 2).

Fig. 3 illustrates Zagros range seismic events (with magnitude $M_w \geq 3$ and depth interval 0-30 km) from *Advanced National Seismic System* for the period January 2007 through January 2009, which are scaled by magnitude. According to this representation, the especially large magnitude earthquakes are restricted to the North Zagros with epicenter at 31.68N 49.93E and along the Zagros Mountain Front Fault with epicenter at 26.87N 54.69E.

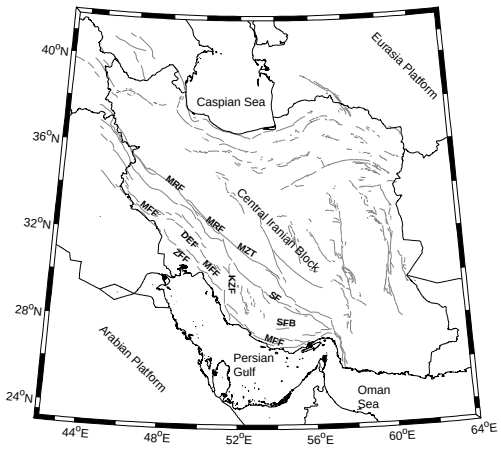

Figure 1: Principal faults of Zagros range. DEF: Dezful Embayment Fault, KZF: Kazerun Fault, MRF: Main Recent Fault, MFF: Mountain Front Fault, MZT: Main Zagros Thrust, SFB: Simple Fold Belt, ZFF: Zagros Fore deep Fault.

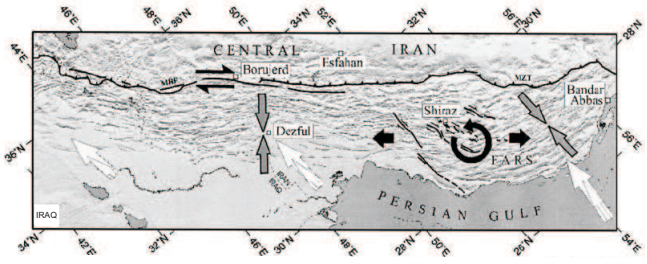

Figure 2: Summary sketch of the tectonic pattern in the Zagros. Overall Arabia-Eurasia motions are shown by the large white arrows (DeMets et al., 1994). Grey arrow couples indicate the general orthogonal shortening, thin black arrows the strike-slip on the MRF, large black arrows along-strike extension due to the Kazerun strike-slip system.

3.1. Iranian permanent GPS network

The *National Cartographic Center of Iran (NCC)* (www.ncc.org.ir) has installed more than 100 permanent stations for monitoring fault movements and earthquake research. This has greatly improved detailed knowledge about the regional and local tectonics in and around Iran. The latest available continuous GPS data around

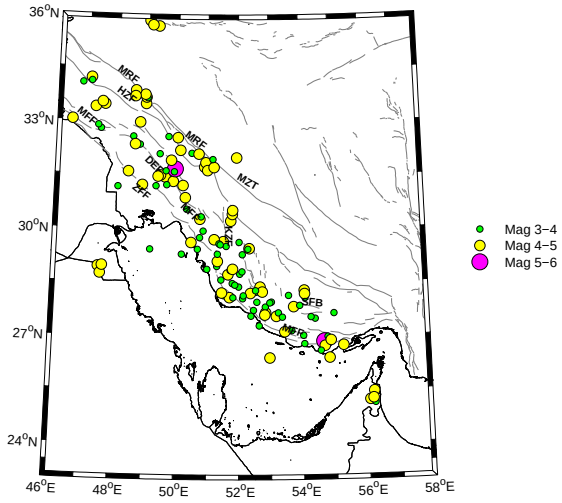

Figure 3: Zagros range seismic events (with magnitude $M_w \geq 3$ and depth interval 0-30 km) from Advanced National Seismic System (ANSS) for the period January 2007 through January 2009, which are scaled by magnitude.

the Zagros region, when this research is undertaken, was from January 2006 through January 2009. Due to the sparsity of the data between the January 2006 through January 2007, which could influence the construction of the Earth's surface as $\mathbb{M}^2$ at continuous time instants, we have chose the daily solutions between January 2007 through January 2009. The solutions are given in the International Terrestrial Reference Frame (ITRF2005). Fig. 4a illustrates the horizontal velocity field along the Zagros range and Fig. 4b represents the vertical velocity field along the Zagros range.

3.2. Analysis and discussion results

The pattern of eigenspace components, namely eigenvalues and eigendirection, of the surface strain-rate tensor and their 95% confidence intervals (in units of 10^{-7} yr^{-1}) is illustrated in the Fig. 5a. Here, we have considered that observations of the random displacement field are independent. The positive eigenvalues are represented by solid lines (red colors) and negative eigenvalues are illustrated by dashed lines (blue colors).

According to our studies, the greatest compression (shortening) is accommodated between the Central Iran block and MRF (triangle SALF-SFHN-ABRK). However, according to our modeling of the displacement field,

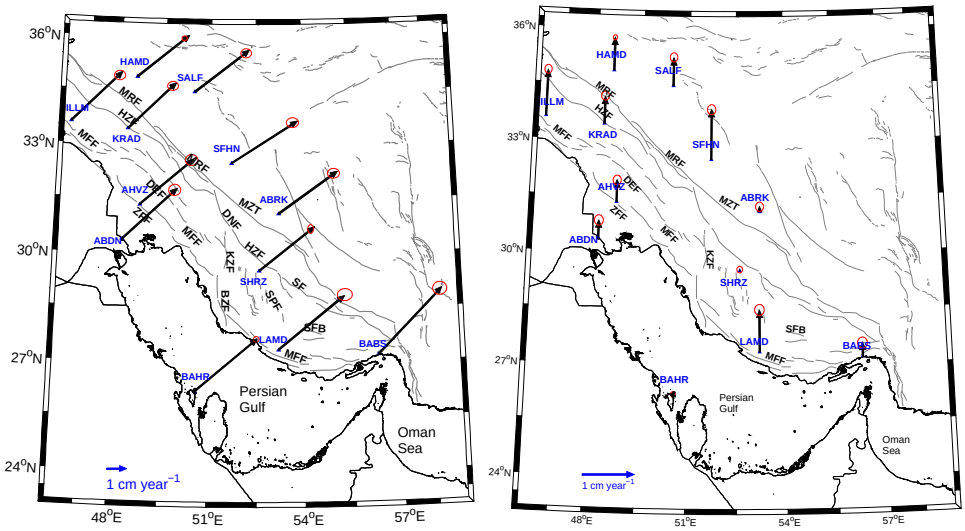

Figure 4: Velocity fields which have nearly daily solutions for the period January 2007 through January 2009 obtained from 11 permanent GPS stations, (a) Horizontal displacements (with 95% confidence ellipses) , (b) vertical displacements.

amount of the deformation could be induced by both of horizontal and vertical motions of the region (see the highest vertical motion of this area which is illustrated in Fig. 4b). Variation of eigendirection in this area is the maximum, which shows variation of direction of deformation across this region. Also, this illustration schematically, describes the oblique shortening along the MFF and SFB.

Most of the extensions occur in the east part of the belt (including stations SHRZ-LAMD-BAHR, SHRZ-SFHN-ABRK and SHRZ-ABRK-BABS). These extensions probably are related to transition between NW Zagros (Borujerd-Dezful) and SE Zagros (Bandar-Abbas). According to Talebian and Jackson (2004), this part rotates in the anticlockwise direction and equipped with strike-slip faults, which took place extension (see Fig. 2).

The estimated eigenspace components of strain tensor based on estimation of covariance matrix of tensor measurements are represented in Fig. 5. A comparison of Figs. 5a and 5b shows that, in general after estimating the covariance matrix of tensor observations, variances of eigenspace components become bigger. The significant variation in localized extension could be seen across the southeastern part of the Zagros, along the Persian Gulf shore (stations SHRZ-LAMD-BAHR), which is bounded by Bandar-Abbas and Dezful. The next variation in extension, is illustrated in Dezful Embayment fault (DEF) nearly parallel to MRF (stations AHVZ-SFHN-KRAD). The significant variations in compressions, are observed along the Mountain Frontal Fault (MFF) which is marked by GPS stations LAMD-BAHR-BABS and NW of the belt illustrated by stations AHVZ-ABDN-ILLM.

In the same manner we illustrated the eigenspace components of TCC and their 95% confidence intervals by Fig. 6. The estimated confidence intervals of eigenvalues and eigendirections of TCC over the Zagros region indicates that deformation is spread over the whole region of the belt from the NW part to the SE part of the Zagros. The pattern shows that the deformation appears with highest positive values across the NW region, nearly in orthogonal direction to the MRF and Main Zagros Fault (MZF). The pattern has insignificant values in the Central Zagros. It takes the significant negative values across the SW part, especially along the Sabz Pushan Fault (SPF) and Persian Gulf shore.

Likewise, we illustrated the eigenspace components of TCC and their 95% confidence intervals, based on es-

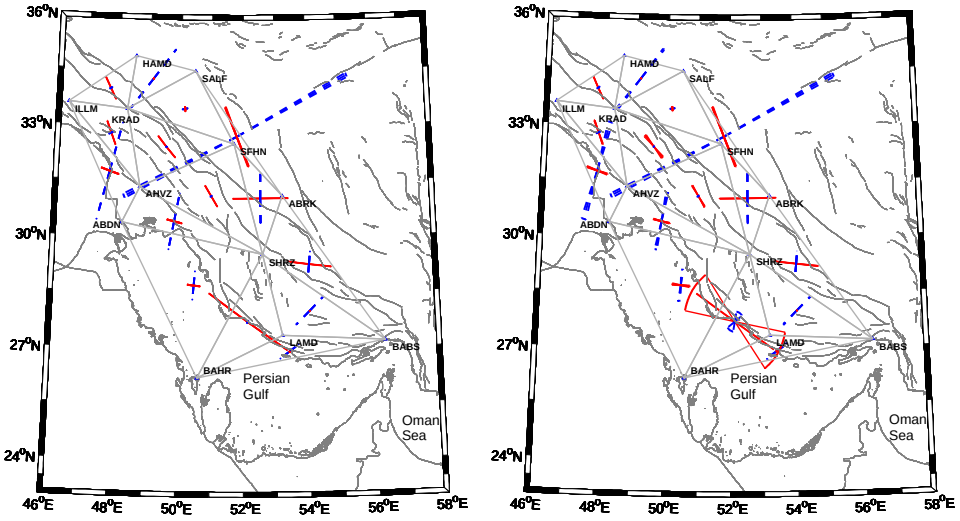

(a) (b)

Figure 5: Pattern of eigenspace components of strain-rate and their 95% confidence intervals, in unit of 10^{-7} yr^{-1}. Extensions are represented by solid lines (red colors) and contractions are illustrated by dashed lines (blue colors). (a) an assumption of independent observations, (b) an assumption of dependency exists between observations.

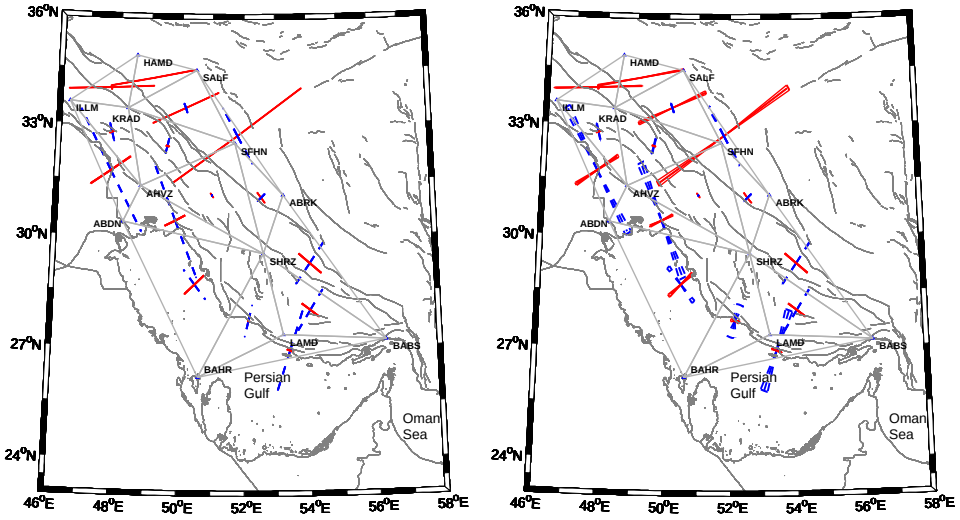

(a) (b)

Figure 6: Pattern of eigenspace components of the TCC and their 95% confidence intervals, in unit of 10^{-8} $\mathrm{m}^{-1}.\mathrm{yr}^{-1}$. Positive eigenvalues are represented by solid lines (red colors) and negative eigenvalues are illustrated by dashed lines (blue colors). (a) an assumption of independent observations, (b) an assumption of dependency exists between observations.

timation of covariance matrix of TCC by Fig. 6b. Comparing Figs. 6a and 6b shows the estimated covariance components have influence on the confidence intervals of eigenspace components.

4. Conclusions

The proposed models are applied by a numerical example with a geodetic network consist of 11 permanent GPS stations around the Zagros region, which have nearly daily solutions (in ITRF 2005) for the period January 2007 through January 2009. According to our studies:

i. Greatest shortening is accommodated in oblique orientation (NS) with respect to the MRF, northwest part of North Zagros, Central Iran block and MRF, respectively. However, according to our modeling of the displacement field, amount of the deformation could be induced by both of horizontal and vertical motions of the region.

ii. Most of the extensions occurred in the east part of the belt. These extensions probably are related to transition between NW Zagros and SE Zagros.

iii. The pattern of eigenspace components of TCC indicates that the highest positive values observed across the NW region, nearly in orthogonal direction to the MRF and MZF. The pattern has insignificant values in the Central Zagros. It takes the significant negative values across the SW part, especially along the SPF and Persian Gulf shore.

iv. The effect of non-independent observations on the estimation of eigenspace components of deformation tensors (strain tensor and TCC) is discussed. It is found that the estimated covariance components have influence on the confidence intervals of eigenspace components, especially in seismically active regions of the belt (along the Persian Gulf shore, NW of the belt and region between the Central Iran block and MRF). They lead to a statement of caution when dealing with data concerning extension and contraction, as well as the orientation of principal stresses.

References

Cai, J., Grafarend, E. W., Schaffrin, B., 2005. Statistical inference of the eigenspace components of a two-dimensional, symmetric rank-two random tensor. Journal of Geodesy 78 (7-8), 425–436.

DeMets, C., Gordon, R. G., Argus, D. F., Stein, S., 1994. Effect of recent revisions to the geomagnetic reversal time scale on estimates of current plate motions. Geophysical Research Letters 21 (20), 21912194.

Grafarend, E., Kleusberg, A., Schaffrin, B., 1980. An introduction to the variance-covariance-component estimation of Helmert type. Z.V.F. 105, 161–180.

Grafarend, E. W., Voosoghi, B., 2003. Intrinsic deformation analysis of the Earth's surface based on displacement fields derived from space geodetic measurements. case studies: present-day deformation patterns of Europe and of the Mediterranean area (ITRF data sets). Journal of Geodesy 77 (5-6), 303–326.

Moghtased-Azar, K., Grafarend, E., 2009. Surface deformation analysis of dense GPS networks based on intrinsic geometry: deterministic and stochastic aspects. Journal of Geodesy 83 (5), 431–454.

Nilforoushan, F., Masson, F., Vernant, P., Vigny, C., Martinod, J., Abbassi, M., Nankali, H., Hatzfeld, D., Bayer, R., Tavakoli, F., Ashtiani, A., Doerflinger, E., Daignires, M., P, P. C., Chry, J., 2003. GPS network monitors the Arabia-Eurasia collision deformation in Iran. Journal of Geodesy 77 (7), 411–422.

Talebian, M., Jackson, J., 2004. A reappraisal of earthquake focal mechanisms and active shortening in the Zagros mountains of Iran. Geophysical Journal International 156 (3), 506–526.

Xu, P. L., Grafarend, E. W., 1996. Probability distribution of eigenspectra and eigendirections of a two-dimensional, symmetric rank two random tensor. Journal of Geodesy 70 (7), 419–430.